Chapter 6

Reactor studies

6.1   Introduction

Studies of future commercial reactors play a useful role in guiding the fusion research and development programme towards an attractive fusion power station. The topics to be addressed for this purpose are safety, environmental friendly operation, and acceptable cost.

In 2000, the European Fusion Programme launched conceptual reactor studies with the objective of specifying the main characteristics of a D-T tokamak reactor and addressing the key issues for availability. Such studies have been classified in three tasks: peak heat flux on the plasma facing materials, blankets, and integration and plant availability [Coo00].

The design provided for these studies is used in this Chapter for evaluating plasma and power plant performance in non-inductive (continuous) operation and comparing them with the reactor objectives. We also carry out a quantitative analysis of the magnitude of synchrotron losses in the power balance of advanced high temperature plasmas envisaged for this commercial reactor. Finally, the optimal confinement enhancement factor which maximizes the plasma amplification factor is discussed.

6.2   Parameters of the plasma reactor

The following nominal geometrical parameters of the European Commercial Reactor [Coo99] are considered:

$$R = 8.1 \,\text{m}, \quad a = 2.7 \,\text{m}, \quad \kappa_{95} = \kappa_X = 1.9, \quad \delta_{95} = \delta_X = 0.4.$$

In our geometrical model, we consider a symmetrical plasma with no X-points (see Fig. 6.1) giving the following poloidal surface S_p, plasma volume V and surface S,

aspect ratio A, and effective elongation κ_a, which are calculated using the expressions introduced in Section 2.6:

$$S_p \simeq 21.8 \text{ m}^2, \quad V \simeq 2170 \text{ m}^3, \quad S \simeq 1259 \text{ m}^2,$$
$$A = 3.1, \quad \kappa_a \simeq 1.74.$$

The toroidal magnetic field on the plasma geometrical axis is

$$B_{t_0} = 6.8 \text{ T}.$$

In Fig. 6.1, we compare the plasma poloidal cross-sections of the M2 device, which has an inductive operating point at $Q = 5$ (see Chapter 5), of ITER-FEAT, which has an inductive operating point at $Q = 10$ (see Chapter 4), and of the commercial reactor considered here, with a nominal operating point in steady-state at $Q \sim 15 - 20$.
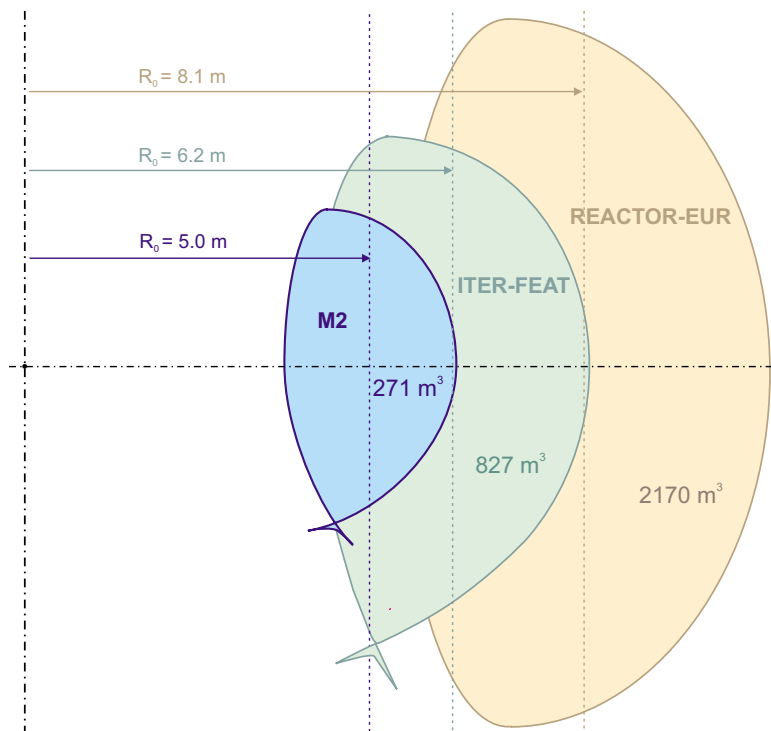

Figure 6.1: Poloidal cross-sections of the plasmas of M2, ITER-FEAT and European Commercial Reactor, and distances from the tokamak axis.

Impurity content are identical to those considered for ITER-FDR [FDR97] ($f_{\text{Be}} = 2\%$, $f_{\text{Ar}} = 0.17\%$), and the helium fraction is calculated self-consistently imposing the ratio of the apparent helium confinement time to the energy confinement time ($\tau_{\text{He}}^*/\tau_E = 5$).

6.3 Global power plant efficiency and electrical power available into the network

According to the power schematic diagram of Fig. 6.2, the electrical power P_{elec} available into the network can be expressed as a function of the fusion power P_{fus}, as follows:

$$P_{\text{elec}} = \frac{P_{\text{fus}}}{Q} \left\{ \eta_{\text{T}} \left[Q \left(1 + \Psi\right) + \frac{1}{\eta_{\text{coup}}} \right] - \frac{1}{\eta_{\text{inj}}\eta_{\text{coup}}} \right\},$$

where η_{T} is the efficiency of the generator of electricity, η_{inj} the electrical efficiency of the power injector including the energizing of the auxiliary equipment, η_{coup} is the fraction of the injected power which is effectively coupled to the plasma ($P_{\text{add}} = \eta_{\text{coup}}P_{\text{inj}}$), and the blanket parameter Ψ is defined as

$$\Psi = f_{\text{n}} \left(M_{\text{B}} - 1\right),$$

where M_{B} is the blanket neutron energy gain, and f_{n} is the fraction of the D-T fusion reaction energy which is kept by the neutrons $f_{\text{n}} = E_n / \left(E_\alpha + E_n\right)$, giving $f_{\text{n}} \simeq 0.8$.

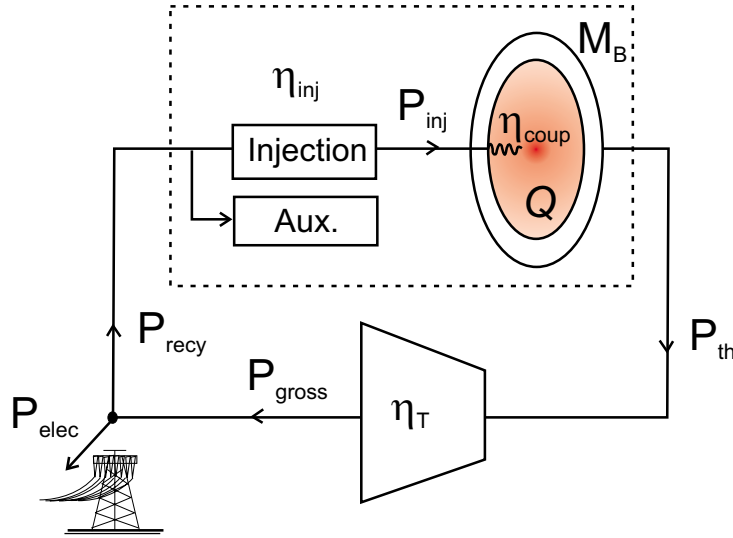Figure 6.2: Schematic diagram of efficiencies and power fluxes of the different elements composing the fusion power plant.

The global efficiency η_{PP} of a thermonuclear power plant is the ratio of the electrical power P_{elec} available into the network to the total nuclear power $P_{\text{nucl}} = P_{\text{fus}} \left(1 + \Psi\right)$ generated within the plant. For given values of the efficiencies of the

different elements composing the power plant the global efficiency η_{PP} is only a function of the plasma amplification factor Q

$$\eta_{PP} = \frac{\eta_T \left[Q \left(1 + \Psi \right) + \frac{1}{\eta_{coup}} \right] - \frac{1}{\eta_{inj} \eta_{coup}}}{Q \left(1 + \Psi \right)}.$$

Another useful parameter is the recycled power fraction f_{recy}, which is the fraction of the gross electrical power P_{gross} required to energize the auxiliary equipments and to inject power into the plasma

$$f_{recy} = \frac{P_{recy}}{P_{gross}}.$$

It can be shown that

$$f_{recy} = \frac{1}{\eta_{inj} \eta_T \left[1 + Q \left(1 + \Psi \right) \eta_{coup} \right]}.$$
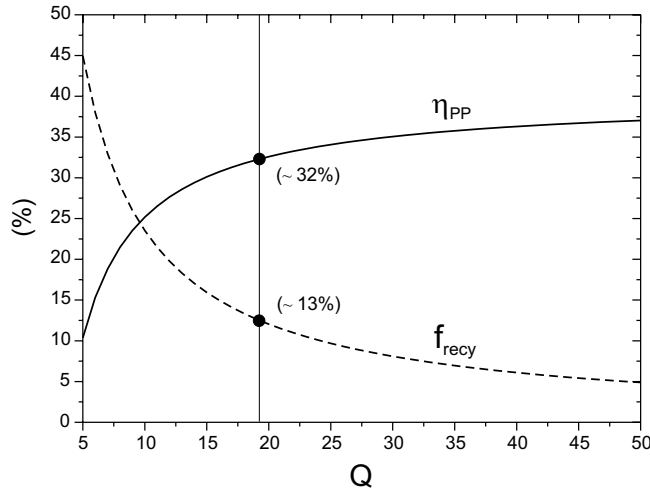

Figure 6.3: global power plant efficiency η_{PP} and recycled fraction f_{recy} versus the plasma amplification factor Q for the following system efficiencies: $\eta_T = 40\%$, $\eta_{inj} = 50\%$, $\eta_{coup} = 90\%$, and $M_B = 1.25$.

In this study we take typical values of efficiencies for the different power plant systems: $\eta_T = 40\%$, $\eta_{inj} = 50\%$, $\eta_{coup} = 90\%$, and $M_B = 1.25$, giving $\Psi \simeq 0.2$. For such values, the evolution of η_{PP} and f_{recy} versus Q is shown in Fig. 6.3. A typical value of global efficiency for present power plants is $\eta_{PP} \sim 33\%$. It could be then

said that $Q \sim 18$ is the minimum value of Q required for a commercial reactor from an economic point of view ($\eta_{PP} > 32\%$, $f_{recy} < 13\%$).

For a given set of reactor and power plant parameters, the cost of electricity decreases when the global power plant efficiency, and consequently the amplification factor Q, increases. Note that for an ignited plasma ($Q = \infty$, $f_{recy} = 0$) we have $\eta_{PP} = \eta_T$, i.e. $\eta_{PP} = 40\%$, for the above values.

6.4 Operation mode and confinement regime

We assume a purely non-inductive mode of operation (no loop voltage, so $P_{OH} = 0$) in which the plasma current is created both by the plasma pressure (bootstrap current) and by a non-inductive current drive method. The efficiency of the current drive method γ_{CD} is supposed to be proportional to the volume average temperature $\langle T_e \rangle$

$$\gamma_{CD} = \gamma_{0CD} \ \langle T_e \rangle \qquad \text{with} \qquad \gamma_{0CD} = 0.2 \times 10^{19}.$$

Such a value of γ_{0CD} has been achieved in experiments carried out on the tokamaks DIII-D [Pet99] and JT-60U [Oik00] using ion cyclotron resonance waves and neutral beam injection, respectively. Note also that higher efficiencies have been reached on the JET tokamak using lower hybrid resonance waves [Eke98], but these waves do not penetrate to the plasma centre under burn conditions. Although simulations performed in the framework of ITER studies show that the temperature proportionality on γ_{CD} is kept for a wide temperature range [Ton94], this is the more restrictive assumption when using this simple model for high-temperature scenarios which are envisaged for a commercial reactor.

In Chapter 4, we have seen that advanced tokamak regimes are required for achieving reasonable thermonuclear plasma performance in non-inductive steady-state operation. Indeed, for the above reactor parameters and assuming an ELMy H-mode confinement regime with a parabolic profile for the electron temperature and with an almost flat profile for the density ($\alpha_n = 0.01$ in Eq. (3.25)), we obtain a maximum amplification factor $Q \simeq 12$, for an operating point satisfying the stability constraints. This point corresponds to an electrical power available into the network of about 1.2 GW, i.e. 20% lower than the nominal value ($P_{elec} = 1.5$ GW) for the European Commercial Reactor [Coo99]. Moreover, the maximum global power plant efficiency is too low ($\eta_{PP} \sim 26\%$) to be economically attractive [Alb00].

Therefore, we consider an advanced tokamak regime with an internal transport barrier characterized by a parabolic density profile. The energy confinement time is $\tau_E = H_H \times \tau_{E,IPB98(y,2)}$, where an enhancement factor $H_H = 1.3$ is taken with respect to the IPB98(y,2) scaling used for the ITER-FEAT design [IPB99]. Such values have been obtained in recent JT-60U high performance discharges near steady-state [Kam00].
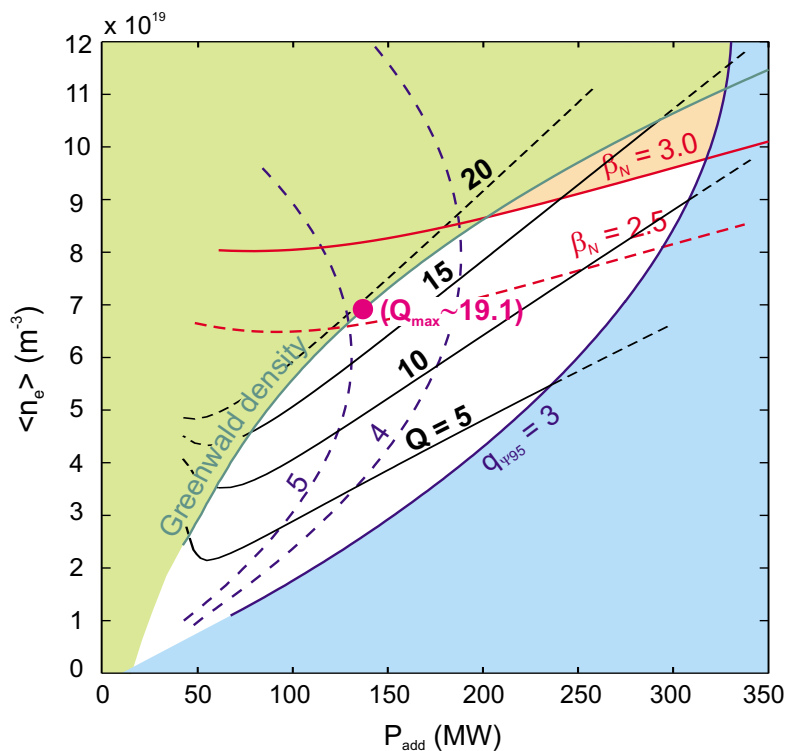
Figure 6.4: Current drive operation diagram (including $q_{\Psi 95}$ iso-contours) for the plasma parameters of the European Commercial Reactor with an advanced confinement regime $H_{\mathrm{H}} = 1.3$ and with a wall reflection coefficient $r = 0.9$.

The temperature profile is described using the radial dependence of Eq. (3.62) with $a_T = 8$, $\beta_T = 5$, and $T_{e_a} = 1$ keV, corresponding to a typical "advanced" temperature profile (displayed in Fig. 4.10). As for the density profile, it is described using a generalized parabolic model (Eq. (3.25)) with $\alpha_n = 1.0$.

The synchrotron losses P_{syn} are calculated using the new fit derived in Section 3.

6.5 Performance analysis

6.5.1 Maximum plasma amplification factor at $r = 0.9$

In Fig. 6.4 we show the current drive operation diagram for a wall reflection coefficient $r = 0.9$. Note first that the effect of wall reflections is estimated using the Trubnikov correction factor $(1 - r)^{1/2}$, and secondly, that $r = 0.9$ is an optimistic value for the wall reflection coefficient. This plot shows iso-contours for $Q = P_{\mathrm{fus}}/P_{\mathrm{add}}$, β_{N}, and $q_{\Psi 95}$ obtained by a self-consistent solution (with the model

described in Chapter 2) of the 0D thermal equilibrium Eq. (2.1) in current drive operation, taking into account both the degradation of the energy confinement time with the non-radiative total power and the imposed value of τ_{He}^*/τ_E.

We observe that the maximum amplification factor is $Q \simeq 19.1$, giving $\eta_{PP} \simeq 32.3\%$ for the power plant system efficiencies taken above[1]. Note that this global power plant efficiency is close to the lowest acceptable value. It can be seen that the highest performance corresponds to an operating point situated at the density limit with a reasonable normalized beta. The safety factor $q_{\Psi95}$ at 95% the magnetic surface is close to 5, corresponding to a total plasma current I_p of about 21 MA.
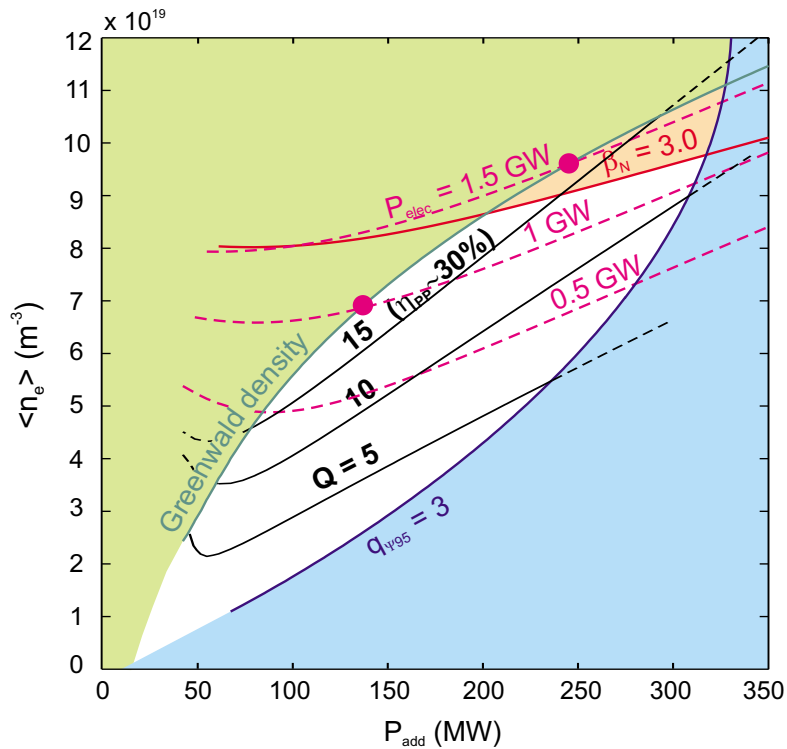

Figure 6.5: Current drive operation diagram (including P_{elec} iso-contours) for the plasma parameters of the European Commercial Reactor with an advanced confinement regime $H_H = 1.3$ and with a wall reflection coefficient $r = 0.9$.

In Fig. 6.5 the iso-contours for the electrical power P_{elec} are added in the current drive diagram for $r = 0.9$. For the highest performance operating point, we obtain $P_{elec} \simeq 1.02$ GW which is lower than the nominal value. To reach the nominal $P_{elec} = 1.5$ GW, the normalized beta must be increased ($\beta_N > 3$) above the limit

---

[1]In this analysis, the highest plasma performance corresponds to the maximum amplification factor Q.

imposed in this study, resulting in a lower amplification factor $Q \sim 16$ and in an additional heating power to be coupled to the plasma around 250 MW. The highest electrical power (on the density and beta limits) is about 1.3 GW.

A fundamental issue in reactor studies concerns the heat flux on the most critical plasma facing components, i.e. the divertor target plates. To treat this problem, we have plotted the iso-contours for $\Phi_{\text{div-peak}}$ in the diagram of Fig. 6.6, when assuming ITER-like physics and technology for the divertor (we use the simple formula (2.13) for the calculation of the peak heat flux on the divertor target plates.). For the highest performance operating point we have a peak heat flux on the divertor target plates higher than 30 MW/m^2, which is much higher than the ITER design value (10 MW/m^2).

The amplification factor at the $\Phi_{\text{div-peak}} = 10$ MW/m^2 point in Fig. 6.6 is reduced to $Q \sim 10$ ($\eta_{\text{PP}} \sim 25\%$), which is unacceptable for a commercial reactor.

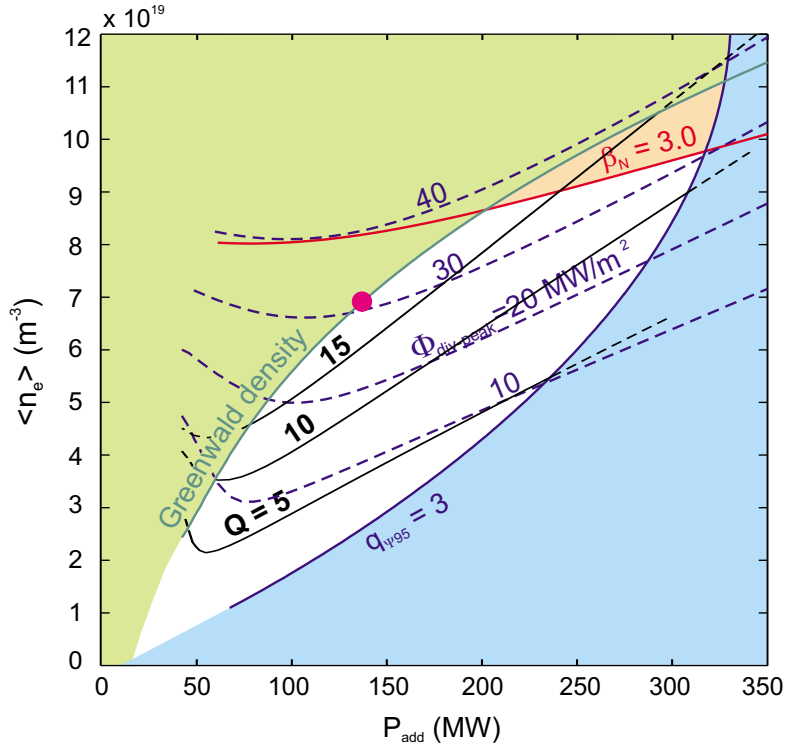Figure 6.6: Current-drive operation diagram (including $\Phi_{\text{div-peak}}$ iso-contours) for the plasma parameters of the European Commercial Reactor with an advanced confinement regime $H_{\text{H}} = 1.3$ and with a wall reflection coefficient $r = 0.9$.

Note that the European reactor study (Ref. [Coo00]) assumes the heat flux profile in the divertor target plates to be spreader than the profile predicted for ITER-FEAT.

This optimistic assumption results in a $\Phi_{\text{div-peak}}$ which is one quarter of that corresponding to an ITER-like heat flux profile on the divertor target plates, when the total power to the divertor is identical. Moreover, the power fraction radiated in the divertor is higher than that of ITER. As a result, a simple law for the $\Phi_{\text{div-peak}}$ containing this different physics in the divertor yields $\Phi^{(1)}_{\text{div-peak}} = 0.11 P_{\text{sep}}/R$, to be compared to the simple law (Eq. (2.13)) used throughout our work ($\Phi_{\text{div-peak}} = 0.62 P_{\text{sep}}/R$). The relevance of such assumptions should be looked at in detail in the European reactor study.

6.5.2 Plasma performance sensitivity to the wall reflection coefficient

To analyse the sensitivity of the plasma performance to the wall reflection coefficient for the synchrotron loss, we look for the highest performance in terms of Q, meeting the requirements for MHD stability ($q_{\Psi 95} \geq 3$, $\beta_N \leq 3$), and density limit ($n_e \leq n_{\text{Greenwald}}$), taking the wall reflection coefficients $r = 0.7$, 0.8, 0.9, and 1.0. Let us notice that $r = 1$ corresponds to the case where synchrotron losses are neglected ($P_{\text{syn}} = 0$) in the thermal plasma equilibrium. Although this is not a realistic case, it has been included as a reference.

The corresponding operating points at highest performance, as well as the ratios of Bremsstrahlung loss, synchrotron loss, and conduction-convection loss to the total losses (i.e. $P_{\text{loss}} = P_{\text{B}} + P_{\text{syn},r} + P_{\text{con}}$), are shown in Table 6.1.

The plasma highest performance in Q is reduced by about 9% when going from $r = 0.9$ to $r = 0.8$, and by about 15% going from $r = 0.9$ to $r = 0.7$. This is due to the growth of the synchrotron loss weight in the plasma power balance when the reflection coefficient decreases (in other words, when the first wall is more transparent to the synchrotron radiation). The decrease of plasma performance is however not dramatic because of the $(1 - r)^{1/2}$ dependence of the wall reflection effect, and due to the fact that the synchrotron power loss is not the dominant loss term. Nevertheless, in all cases the synchrotron losses are significant in the global power balance, representing 17% of the total power losses for $r = 0.9$, 21% for $r = 0.8$, and 24% for $r = 0.7$.

Note that this important conclusion is different from that of previous studies (see, for example, Ref. [Bor83]). The reason is that we consider different plasma parameters for the reactor (higher magnetic field and plasma elongation), that the temperatures required for high Q operation in current drive are also higher (~ 50 keV at the magnetic axis), and that we take into account the strong temperature profile effect illustrated in Chapter 3.

In this quantitative application, since the highest performance point of the plasma with the reference reflection coefficient (at $r = 0.9$) is close to the minimum value of η_{PP} acceptable for a commercial reactor, the design of a first wall maximizing such

Table 6.1: Highest performance operating point for a D-T reactor plasma in current drive operation, with a wall reflection $r = 0.7$, $r = 0.8$, $r = 0.9$ and $r = 1$.

	$r = 0.7$	$r = 0.8$	$r = 0.9$	$r = 1.0$
Q	16.2	17.3	19.1	25.7
T_{e_0} (keV)	42.7	44.3	46.8	54.1
$\langle T_e \rangle$ (keV)	16.0	16.7	17.6	20.4
n_{e_0} (10^{20} m^{-3})	1.30	1.33	1.38	1.50
$\langle n_e \rangle$ (10^{20} m^{-3})	0.65	0.67	0.69	0.76
$q_{\Psi 95}$	5.12	4.99	4.81	4.41
I_p (MW)	19.8	20.3	21.1	23.0
f_{BS} (%)	57.3	58.0	59.1	62.6
f_{He} (%)	11.3	11.4	11.6	11.6
P_B/P_{loss} (%)	12	12	12	13
P_{syn}/P_{loss} (%)	24	21	17	0
P_{con}/P_{loss} (%)	64	67	71	87
P_{loss} (MW)	593	622	669	799
P_{add} (MW)	139	138	137	129
P_{fus} (MW)	2240	2390	2630	3310
β_N	2.37	2.46	2.59	3.0
P_{elec} (MW)	830	902	1020	1360
η_{PP} (%)	30.8	31.4	32.3	34.2
$\Phi_{div\text{-}peak}$ (MW/m^2)	24	27	31	47

a coefficient becomes crucial. Note that, as seen in Table 6.1, both the global power plant efficiency and the electric power available to the network, decrease when r decreases.

In contrast to the behaviour observed for $r = 0.7$, 0.8, and 0.9, in the case $r = 1$ the amplification factor increases steadily with the normalized beta, and thus the highest performance is situated at the intersection of Greenwald density and beta limit ($\beta_N = 3.0$). For this point, we obtain an amplification factor $Q \sim 26$, which is substantially higher than those obtained with realistic reflection coefficient ($r < 1$). Therefore, the fact of considering or not synchrotron losses in the global plasma balance has important consequences on the plasma performance.

6.5.3 The role of the current drive efficiency

Up to now in this Chapter, the current drive efficiency is supposed to be proportional to the volume average temperature with a proportionality value $\gamma_{0CD} = 0.2 \times 10^{19}$. Figs 6.7, 6.8, and 6.9 show the iso-contours $q_{\Psi 95}$, P_{elec}, and $\Phi_{div\text{-}peak}$,

respectively, in the current drive diagram of the European Commercial Reactor obtained with a wall reflection coefficient $r = 0.9$, when γ_{0CD} is taken to be 0.35×10^{19}. This latter value of γ_{0CD} is considered in some reactor studies, as for example in Ref. [Tos00], which are less conservative than our study.
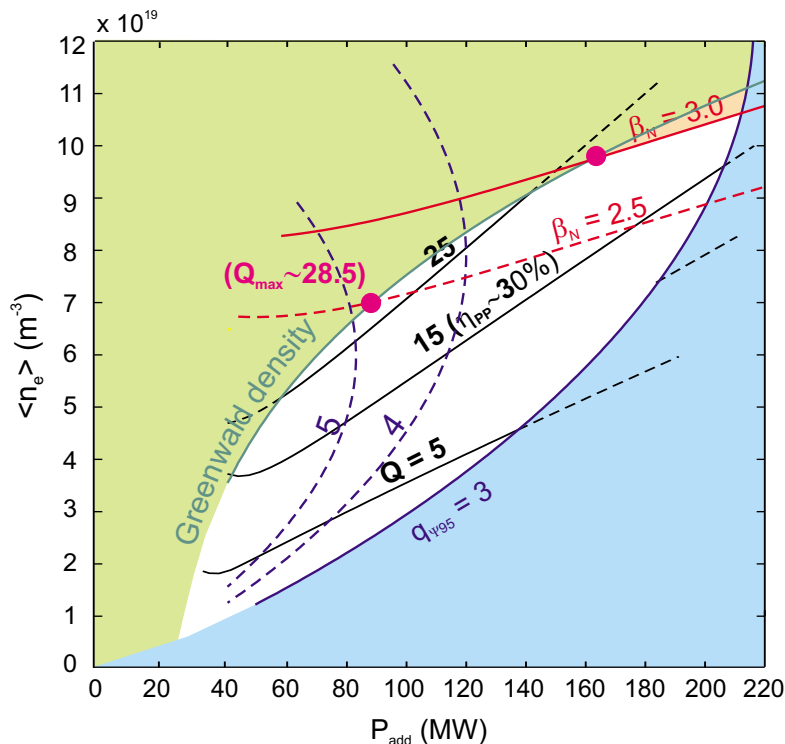

Figure 6.7: Current drive operation diagram (including $q_{\Psi95}$ iso-contours) for the plasma parameters of the European Commercial Reactor with $\gamma_{0CD} = 0.35 \times 10^{19}$, with an advanced confinement regime $H_H = 1.3$, and with a wall reflection coefficient $r = 0.9$.

The main results from Figs 6.7, 6.8 and 6.9 are as follows. First of all, the maximum amplification factor using $\gamma_{0CD} = 0.35 \times 10^{19}$ is $Q \simeq 28.5$, giving $\eta_{PP} \sim 35\%$ for the power system efficiencies considered in this study. These values are significantly higher than those obtained with $\gamma_{0CD} = 0.2 \times 10^{19}$, due to a higher plasma current which improves the confinement and makes the density and beta limits larger. The P_{elec} for this highest performance operating point is about 1 GW, lower again than the nominal value.

Secondly, there is a second operating point located at the intersection of the $n/n_{Gr} = 1$ and $\beta_N = 3$ curves, which has a reasonable amplification factor $Q \sim 23$ ($\eta_{PP} \sim 33\%$), providing the requested electrical power into the network ($P_{elec} \sim 1.5$ GW). Finally, let us note that despite the peak heat fluxes on the divertor target plates
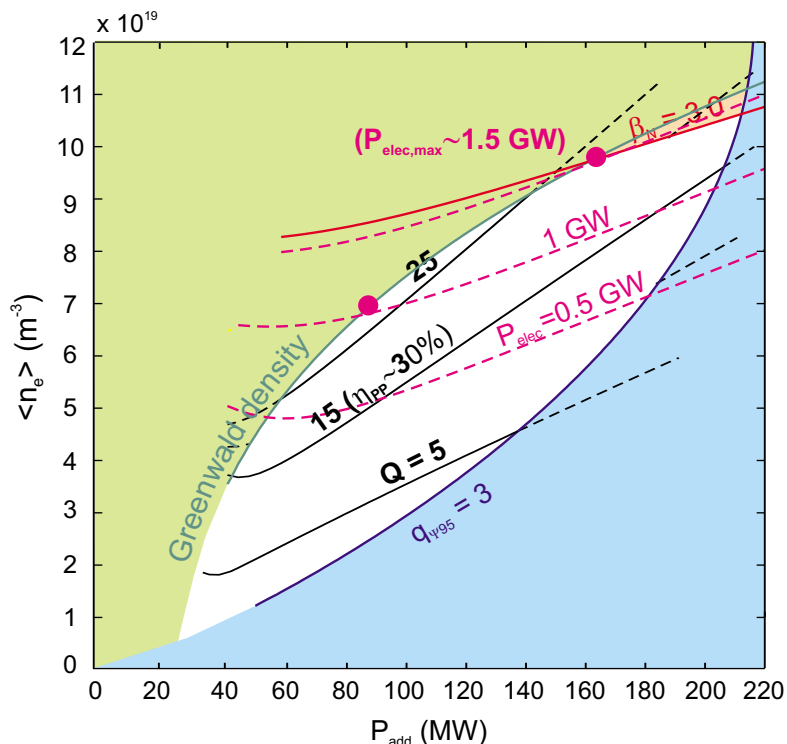
Figure 6.8: Current drive operation diagram (including P_{elec} iso-contours) for the plasma parameters of the European Commercial Reactor with $\gamma_{0CD} = 0.35 \times 10^{19}$, with an advanced confinement regime $H_H = 1.3$, and with a wall reflection coefficient $r = 0.9$.

for these points are higher again than the ITER design value (see Fig. 6.6), they are lower (by 30%) than those of the current drive diagram with $\gamma_{0CD} = 0.2 \times 10^{19}$ (see Fig. 6.9).

We conclude that the growth of the current drive efficiency improves the plasma performance, increases the fusion and electrical power, and decreases the heat load on the plasma facing components (e.g. on the divertor).

6.6 Optimal confinement enhancement factor H_H

6.6.1 Optimisation of Q versus the optimisation of H_H

In order to minimize the cost of electricity, and consequently to make fusion energy more competitive, we must obtain both a high plasma performance in Q and a high enough electrical power into the network.
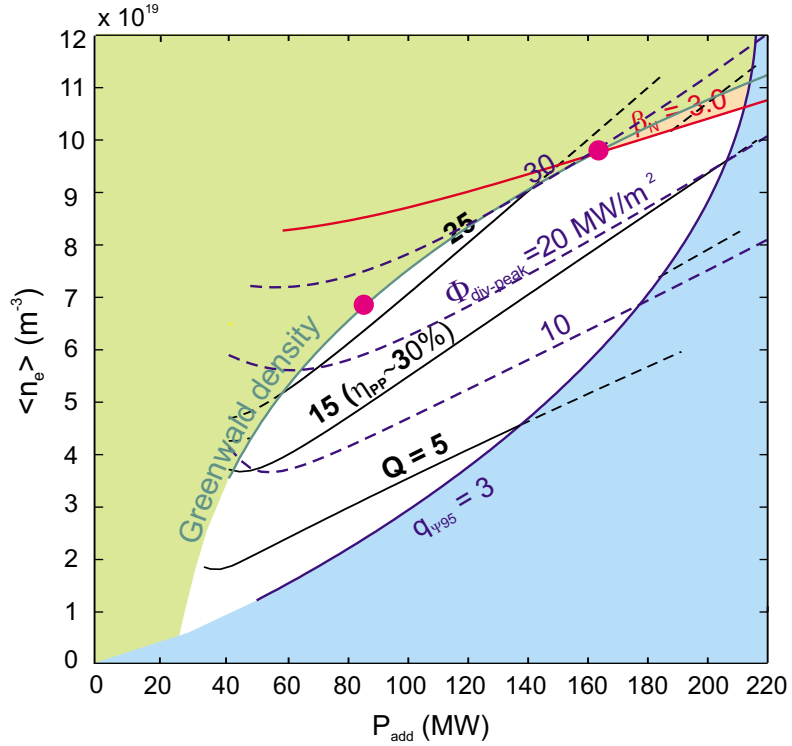
151

Figure 6.9: Current drive operation diagram (including $\Phi_{\text{div-peak}}$ iso-contours) for the plasma parameters of the European Commercial Reactor with $\gamma_{0\text{CD}} = 0.35 \times 10^{19}$, with an advanced confinement regime $H_{\text{H}} = 1.3$, and with a wall reflection coefficient $r = 0.9$.

It could be thought that these conditions are met when the plasma confinement is improved, i.e. when the confinement enhancement factor H_{H} is maximum, but, whereas the maximum amplification factor Q meeting the MHD plasma requirements increases steadily when H_{H} increases, the highest electrical power meeting the same requirements decreases steadily (see Fig. (6.10)). Moreover, the point of maximum amplification factor and the point of highest electrical power are not the same point in the current drive diagram (see, for example, Fig. 6.5). Both points are located on the Greenwald density curve, but the first has an intermediate normalized beta whilst the second one is located on the normalized beta limit. Consequently, the operating point at highest electrical power does not have the highest performance. This effect will be explained below by means of analytical expressions (see Section 6.6.2).

In Fig. 6.10, we show the evolution of Q and P_{elec} as a function of the H_{H} factor, for the operating points at highest plasma performance in Q (left side) and for the operating points at highest electrical power into the network (right side). We observe
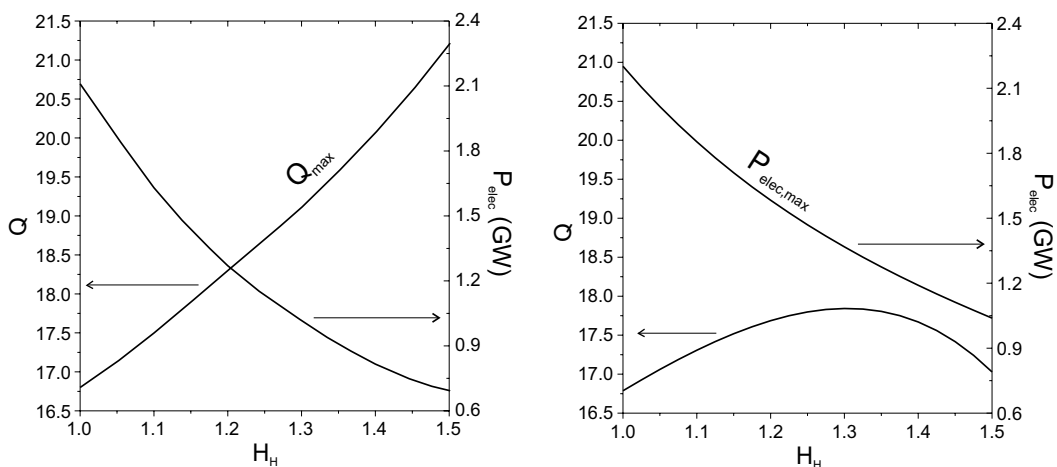
Figure 6.10: Amplification factor Q and electrical power P_{elec} at the Greenwald density limit versus the confinement enhancement factor H_H, for the operating points at highest plasma performance in Q (on the left side), and for the operating points at highest electrical power on the network $P_{elec,max}$ (on the right side).

that the plasma performance in Q corresponding to the highest electrical power not only increases less than Q_{max} when H_H increases, but also it reaches a maximum (at $H_H \sim 1.3$) which is followed by a roll-over of Q when the confinement enhancement factor is still increased.

Therefore, the optimal confinement enhancement factor H_H for a reactor is not necessarily the highest. Indeed, we could try to find out the optimal enhancement factor when the electrical power is imposed to $P_{elec} = 1.5$ GW. As seen in Fig. 6.11, the amplification factor in this case (at $n/n_{Gr} = 1$ and $P_{elec} = 1.5$ GW) has a maximum $Q \sim 18$ at an intermediate enhancement factor $H_H \sim 1.2$. We also see that for higher H_H factors, the plasma pressure is larger than the beta limit. On the other hand, the peak heat flux on the divertor increases when the enhancement factor H_H decreases.

6.6.2 Analytical expressions when imposing the density and the normalized beta limits

In this Section, we analyse in detail the unexpected behaviour of the Q curve as a function of the enhancement factor H_H shown in the previous Section, considering the plasma in non-inductive mode of operation at the density limit and normalized beta limit (i.e. at the point giving the highest electrical power), and using the parametric expressions of the plasma model described in Chapter 2.
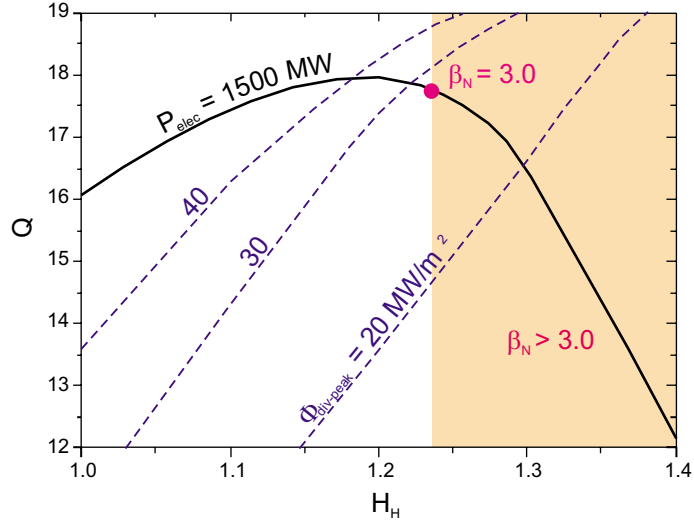
153

Figure 6.11: Amplification factor Q at the Greenwald density limit versus the confinement enhancement factor H_H, for the $P_\text{elec} = 1.5$ GW curve and $\Phi_\text{div-peak}$ iso-contours.

In this study, we assume a set of reactor parameters (R, a, κ, δ, B_t), with a given shape for the density and temperature profiles (α_n, α_T, β_T, θ_i), with a current drive efficiency proportional to the temperature, with impurity species Z_1 and Z_2 of fraction f_1 and f_2, and with a constant ratio τ_He^*/τ_E of the apparent helium confinement time to the energy confinement time.

For each value of H_H, we must solve the following equations for the density n_{e_0} at the magnetic axis, the temperature T_{e_0} at the magnetic axis, the total plasma current I_p, the bootstrap current fraction f_BS, and helium fraction f_He:

- The density limit can be expressed from Eq. (2.24) as a relation between the plasma current and density

$$I_p = C_\text{Gr} n_{e_0}, \tag{6.1}$$

where C_Gr is a constant for a given set of reactor parameters.

- For a given normalized beta limit ($\beta_\text{N} = \beta_\text{Nmax}$), the density, temperature, plasma current and helium fraction are related by Eq. (2.26) as follows:

$$T_{e_0} = C_\beta \frac{I_p}{C_W\left(f_\text{He}\right) n_{e_0}}, \tag{6.2}$$

where C_W is the multispecies coefficient (depending on f_He) given in Eq. (2.12), and C_β is a constant for a given set of reactor parameters. Making the substitution of Eq. (6.1) in Eq. (6.2), we obtain the temperature at the magnetic axis

154

as a function of the helium fraction

$$T_{e_0} = \frac{C_\beta C_{\text{Gr}}}{C_W\left(f_{\text{He}}\right)}. \tag{6.3}$$

- The plasma current in the non-inductive mode of operation is made up of the current I_{CD} driven by the additional power P_{add} and the bootstrap current I_{BS}. The first one ($I_{\text{CD}} = (1 - f_{\text{BS}})\,I_p$) is related to P_{add} by means of the efficiency γ_{CD} (Eq. (2.35).) Expressing $P_{\text{add}} = P_{\text{ext}}$ ($P_{\text{OH}} = 0$ in non-inductive operation mode) as a function of the amplification factor Q and P_α

$$P_{\text{add}} = C_5 P_\alpha / Q$$

with the constant C_5 given in Eq. (2.6) and P_α given in Eq. (2.4), and according to Eq. (6.1), it can be seen that

$$Q = \frac{C_5}{C_{\text{Gr}} R}\frac{C_\alpha\left(f_{\text{He}}\right)\,\gamma_{\text{CD}}\left(T_{e_0}\right)\,\overline{\sigma v}^*_{\text{DT}}(T_{e_0})}{\left(1 - f_{\text{BS}}\right)}, \tag{6.4}$$

where C_α is the dilution coefficient given in Eq. (2.2) and $\overline{\sigma v}^*_{\text{DT}}$ is the D-T thermonuclear reaction rate.

- The bootstrap current fraction (Eq. (2.36)) on the density limit (Eq. (6.1)) and normalized beta limit (Eq. (6.2)) can be expressed as

$$f_{\text{BS}} = \frac{C_{\beta_p} C_\beta}{C_{\text{Gr}}}\frac{B\left(f_{\text{He}}\right)}{n_{e_0}}, \tag{6.5}$$

where C_{β_p} is a constant for a given set of reactor parameters, and the constant B is given in Ref. [Wil92]. Note that this fraction does not depend on the temperature.

- The thermal equilibrium equation (Eq. (2.1)) is solved by calculating the conductive-convective losses ($P_{\text{con}} = P_{\text{net}} = (1 + C_5/Q)\,P_\alpha - P_{\text{B}} - P_{\text{syn}}$) from a monomial scaling law for the global energy confinement time, which for a given reactor can be written as

$$\tau_E = H_{\text{H}} \times C_\tau \frac{I_p^{x_I}\,n_{e_0}^{x_n}}{P_{\text{net}}^{x_P}},$$

where $P_{\text{net}} = P_{\text{con}} = (1 + C_5/Q)\,P_\alpha - P_{\text{B}} - P_{\text{syn}}$, and C_τ is a constant for a given set of reactor parameters. Expressing the plasma energy content as $W_{\text{th}} = C_W^{(0)} C_W\left(f_{\text{He}}\right) n_{e_0} T_{e_0}$, and according to the density limit and normalized beta limit equations (6.1) and (6.2), it can be shown that

$$P_{\text{net}}^{1-x_P} = \frac{C_\beta C_W^{(0)} C_{\text{Gr}}^{1-x_I}}{H_{\text{H}} C_\tau} n_{e_0}^{1-x_n-x_I}. \tag{6.6}$$

- According to the ratio $\tau_{\text{He}}^*/\tau_E$ of the apparent helium confinement time to the energy confinement time defined in Eq. (2.34), and to the density limit and normalized beta limit conditions (Eqs (6.1) and (6.2)), it can be seen that

$$\frac{\tau_{\text{He}}^*}{\tau_E} = \frac{C_t}{H_{\text{H}}^{\frac{1}{1-x_P}}} \frac{f_{\text{He}}}{n_{e_0}^{\frac{x_1}{1-x_P}} C_\alpha\left(f_{\text{He}}\right) \overline{\sigma v}_{\text{DT}}^*(T_{e_0})}, \tag{6.7}$$

with $x_1 = 1 + x_n + x_I - 2x_P$ and

$$C_t = \frac{E_\alpha V \, C_\beta^{\frac{x_P}{1-x_P}} C_W^{(0)\frac{x_P}{1-x_P}} C_{\text{Gr}}^{\frac{x_P-x_I}{1-x_P}}}{C_\tau^{\frac{1}{1-x_P}}},$$

where E_α is the initial kinetic energy of the alpha particle.

Sensitivity study of the confinement enhancement factor for a given f_{He}:

As a first approach, the helium fraction f_{He} is assumed to be constant. In this case, imposing both the density and the normalized beta limits (Eq. (6.3)), the temperature T_{e_0} at the magnetic axis (and hence the volume averaged temperature $\langle T_e \rangle$ and $\overline{\sigma v}_{\text{DT}}^*$) is kept constant for any value of the enhancement factor H_{H}.

Then, it can be shown that Eq. (6.4) becomes

$$Q = \frac{C_{q_0}}{1 - f_{\text{BS}}} \tag{6.8}$$

with

$$C_{q_0} = \frac{C_5 C_\alpha \, \gamma_{\text{CD}} \, \overline{\sigma v}_{\text{DT}}^*}{C_{\text{Gr}} \, R}.$$

According to Eq. (6.8), the dependence of the amplification factor versus the enhancement factor in this case is determined by the bootstrap current fraction. Since the bootstrap fraction increases when the poloidal beta increases (see Eq. (2.36)) and, at the density and the normalized beta limits, the poloidal beta increases when the plasma current (and hence the density) decreases (as seen in Eq. (6.5)), we conclude that the amplification factor increases when the density decreases,

$$Q = \frac{C_{q_0}}{1 - C_{\text{BS}_0}/n_{e_0}} \tag{6.9}$$

with

$$C_{\text{BS}_0} = \frac{C_{\beta_p} C_\beta \, B}{C_{\text{Gr}}}.$$

Next, we analyse the dependence of H_{H} on n_{e_0} for the special case of a non-radiative plasma and the realistic case of a radiative plasma.

Case of a non-radiative plasma

In the special case of a non-radiative plasma, we have $P_B = P_{syn} = 0$, and $P_{net} = P_\alpha + P_{add}$. In such a case, Eq. (6.6) becomes

$$H_H = \frac{C_{H_0}}{n_{e0}^{x_1} \left[1 + \frac{C_5}{C_{q0}}\left(1 - C_{BS_0}/n_{e0}\right)\right]^{1-x_P}}, \tag{6.10}$$

and taking into account Eq. (6.9), we obtain the following expression for H_H as a function of Q:

$$H_H = \frac{C_{H_0}}{C_{BS_0}^{x_1}} \frac{\left(1 - C_{q0}/Q\right)^{x_1}}{\left(1 + C_5/Q\right)^{1-x_P}}, \tag{6.11}$$

with

$$C_{H_0} = \frac{C_\beta C_W^{(0)} C_{Gr}^{1-x_I}}{C_\tau C_\alpha^{1-x_P} \overline{\sigma v}_{DT}^{*1-x_P}}.$$

Note that $x_1 > 0$ in the monomial scaling laws for the global energy confinement time. From Eqs (6.10) and (6.11) we conclude that, for a given helium fraction, the plasma density decreases when the enhancement factor H_H increases. As a result, the amplification factor increases.
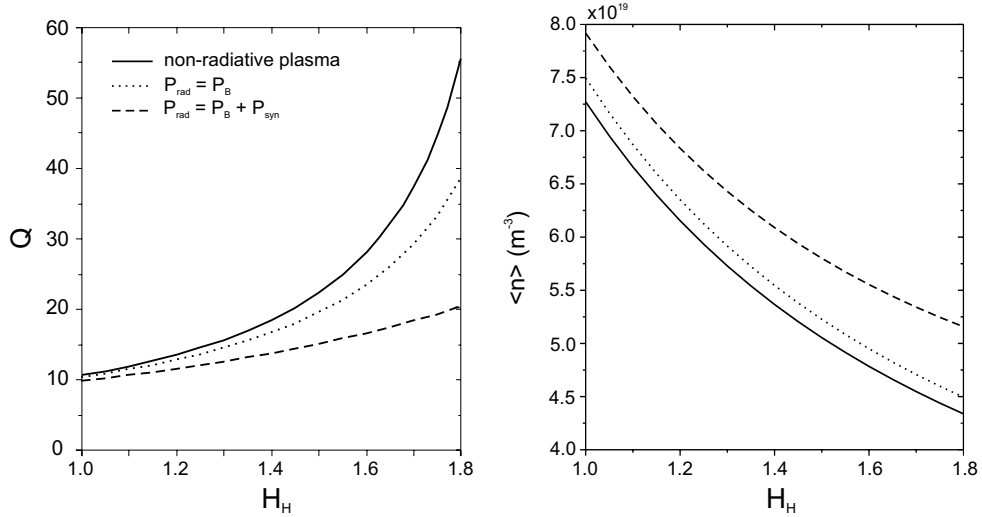

Figure 6.12: Q factor and volume averaged density $\langle n \rangle$ versus the confinement enhancement factor H_H for a non-radiative plasma (solid line), a Bremsstrahlung radiative plasma (dotted line), and a complete (Bremsstrahlung and synchrotron losses) radiative plasma (dashed line), when the Helium fraction f_{He} is imposed.

Case of a radiative plasma

Modelling the Bremsstrahlung loss with Eq. (2.7) and synchrotron loss with the new fit proposed in Chapter 3 (Eq. (3.67)) leads to the following expression relating the enhancement factor H_H and the density n_{e_0}:

$$H_\mathrm{H} = \frac{C_{H_0}}{n_{e_0}^{x_1} \left[1 + \frac{C_5}{C_{q_0}} \left(1 - C_{\mathrm{BS}_0}/n_{e_0} \right) - C_{\mathrm{B}_0} - C_{s_0} \dfrac{n_{e_0}^{-1.76}}{\left(C_{s_1} + n_{e_0}^{0.41} \right)^{1.51}} \right]^{1-x_P}},$$

with

$$C_{\mathrm{B}_0} = \frac{C_\mathrm{B} Z_\mathrm{eff} C_\beta^{1/2} C_\mathrm{Gr}^{1/2}}{C_W^{1/2}}, \quad C_{s_0} = \frac{C_s C_\beta^{5/2} C_\mathrm{Gr}^{5/2}}{C_W^{5/2}},$$

$$C_s = P_\mathrm{syn} \frac{\left(C_{s_1} + n^{0.41} \right)^{1.51}}{n_{e_0}^{0.24}}, \quad \text{and} \quad C_{s_1} = \frac{5.36 \times 10^5 T_{e_0} B_{t_0}^{0.41}}{a^{0.41}}.$$

which are constant for a given set of reactor parameters and temperature. In Fig. 6.12, we show the amplification factor and the volume averaged density (in the radiative and non-radiative cases) for different values of H_H, considering the ELMy H-mode IPB98(y,2) scaling law for the energy confinement time [IPB99] ($x_P = 0.69$, $x_n = 0.41$, $x_I = 0.93$) and the parameters of the European Commercial Reactor with a fixed $f_\alpha = 10\%$, and $\alpha_n = 1$, $\alpha_T = 8$, $\beta_T = 5$.

Due to the n_e^2 dependence on Bremsstrahlung losses, the density versus H_H has the same trend as the non-radiative case when this term is added. Concerning the synchrotron loss term, it adds a new term in density which modifies the dependence $H_\mathrm{H} = f(n_e)$, causing the density to decrease more slowly than in the non-radiative case. The rise of Q with H_H is thus lower in this case, as seen in Fig. 6.12.

Note that for a fixed helium fraction, when H_H increases, the temperature is constant and the density decreases for increasing values of H_H. Consequently, the fusion power and the electrical power into the network also decrease.

Q saturation with increasing H_H for a given ratio $\tau_\mathrm{He}^*/\tau_E$:

When the ratio $\tau_\mathrm{He}^*/\tau_E$ of the apparent helium confinement time to the energy confinement time is imposed, the helium fraction varies with the enhancement factor H_H.

In Fig. (6.13) we show the behaviour of the (a) amplification factor Q, (b) ratio of synchrotron loss to the total loss $P_\mathrm{syn}/P_\mathrm{loss}$, (c) central electron density n_{e_0} (d) central electron temperature T_{e_0}, (e) helium fraction f_He, and (f) bootstrap current fraction f_BS when varying the confinement enhancement factor H_H.

In this case, the following sequence of events is produced when the enhancement factor increases. First of all, as the ratio $\tau_\mathrm{He}^*/\tau_E$ is kept constant, the helium fraction
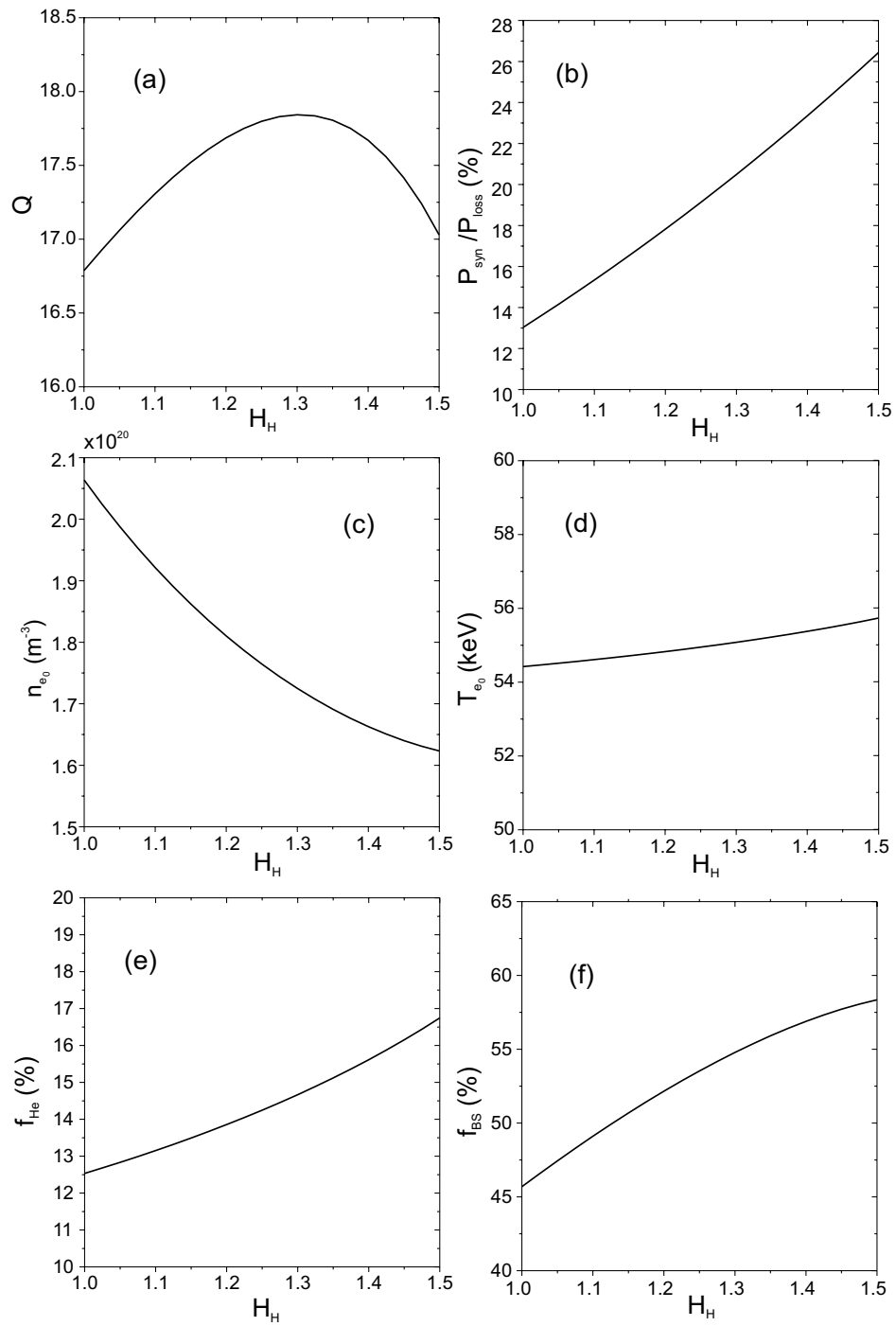
Figure 6.13: Dependences on the enhancement factor H_H at the density and beta limits when imposing $\tau_{He}^*/\tau_E = 5$.

increases in order to compensate for the growth of the energy confinement time. Secondly, according to Eq. (6.3), the temperature slightly increases. Next, Eq. (6.7) leads to

$$n_{e_0} = \frac{C_t^{\frac{1-x_P}{x_1}}}{H_{\mathrm{H}}^{1/x_1} \left(\tau_{\mathrm{He}}^*/\tau_E\right)^{\frac{1-x_P}{x_1}}} \frac{f_{\mathrm{He}}^{\frac{1-x_P}{x_1}}}{\left(P_\alpha/n_{e_0}^2\right)^{\frac{1-x_P}{x_1}}}, \qquad (6.12)$$

where $P_\alpha/n_{e_0}^2$ depends on the temperature and on the helium fraction. There are two competing effects in the alpha heating power: on one hand, the D-T reactivity increases with the temperature, which slightly grows with H_{H}. On the other hand, the dilution effect (see Chapter 2) causes a contrary effect due to the rise of the helium fraction, which increases with H_{H}. It is seen that the dilution effect is the dominant one. The combination of all the events makes the density steadily to decrease when the enhancement factor H_{H} increases (as in the case where the helium fraction is imposed). Finally, the bootstrap fraction increases with H_{H} (Eq. (6.5)), and the amplification factor is expressed as the addition of the above effects, as seen in Eq. (6.4) and in the following expression derived from Eqs (6.6) and (6.7):

$$\frac{C_5}{Q} = \frac{P_{\mathrm{B}}}{P_\alpha} + \frac{P_{\mathrm{syn}}}{P_\alpha} + \frac{C_q}{f_{\mathrm{He}}} - 1$$

with

$$C_q = \frac{C_\beta^{\frac{1}{1-x_P}} C_{\mathrm{Gr}}^{\frac{1-x_L}{1-x_P}} C_W^{(0)\frac{1}{1-x_P}} \left(\tau_{\mathrm{He}}^*/\tau_E\right)}{C_\tau^{\frac{1}{1-x_P}} C_t}.$$

In Fig. (6.13) we see that the highest amplification factor Q on the density and beta limits ($Q \simeq 17.8$) corresponds to $H_{\mathrm{H}} \sim 1.3$.

We conclude that when the enhancement factor increases, there is a competition for the plasma performance between one favourable effect (bootstrap fraction increases) and two unfavourable effects (the weight of synchrotron losses increases, and the dilution effect becomes more significant when f_{He} increases). For the set of parameters and conditions considered, Q would increase without only one of these unfavourable effects.

Let us notice that the same study has been performed with a constant current drive efficiency $\gamma_{0\mathrm{CD}}$ (do not depending on temperature) and a similar behaviour is obtained.

6.7 Summary

The analysis of the performance of the European Commercial Reactor shows that, using values of current drive efficiency and of confinement enhancement factor in agreement with present-day experiments, the highest plasma performance is $Q \sim 19$ (giving a marginally acceptable global power plant efficiency $\eta_{PP} \sim 32\%$) and the highest electrical power into the network is about 1.3 GW (lower than the 1.5 GW nominal value), despite the optimistic value taken for the wall reflection coefficient ($r = 0.9$) for synchrotron radiation.

Assuming an ITER-like physics and technology for the divertor, the peak heat flux on the divertor target plates $\Phi_{\text{div-peak}}$ for the above operating points is higher than 30 MW/m^2, much larger than the ITER design value (10 MW/m^2). Therefore, the physics and technology of the divertor of this reactor should be significantly improved with respect to the ITER-like one.

Assuming a higher current drive efficiency the plasma performance is improved, the fusion power and the electrical power is increased, and the heat load on the plasma facing components is decreased. In particular, the nominal values of electrical power into the network for the European Commercial Reactor ($P_{\text{elec}} = 1.5$ GW) with acceptable global power plant efficiency ($Q \sim 23$, $\eta_{PP} \sim 33\%$) and meeting the stability requirements are achieved in the case $\gamma_{0CD} = 0.35 \times 10^{19}$, which is considered in other less conservative reactor studies.

Taking into account the temperature profile effects, we have illustrated that synchrotron losses become significant in the advanced high temperature plasmas ($T_{e_0} \sim 50$ keV) envisaged for this reactor in non-inductive operation. In all the cases considered, this term represents approximately 20% of the total losses. It has been shown that the plasma performance is quite sensitive to the value of the wall reflection coefficient (e.g. the highest Q is reduced by about 15% when going from $r = 0.9$ to $r = 0.7$).

Due to synchrotron losses (increased in "advanced" profiles required for achieving reasonable thermonuclear plasma performance) and to the experimentally observed conservation of the ratio of the apparent helium confinement time to the energy confinement time, there is an optimal confinement enhancement factor H_H which maximizes the plasma performance in Q corresponding to a given electrical power into the network (e.g. 1.5 GW) or to the highest electrical power meeting the MHD plasma requirements. For the point of highest electrical power, which is located on the density and beta limits, it has been shown that when the enhancement factor increases, there is a competition for the plasma performance between one favourable effect (bootstrap fraction increases) and two unfavourable effects (the ratio of synchrotron loss to the total loss increases, and the dilution effect becomes more significant). As a result, the amplification factor Q on the density and beta limits reaches a maximum (at $H_H \sim 1.3$) which is followed by a roll-over of the

plasma performance when the confinement enhancement factor is still increased.

The maximum in the Q curve versus the confinement enhancement factor H_{H} is only produced when the ratio $\tau_{\mathrm{He}}^{*}/\tau_{E}$ of the apparent helium confinement time to the energy confinement time is imposed, and when synchrotron losses are considered in the global thermal balance. This effect is important because we are looking for both a high plasma performance and a high enough electrical power into the network, in order to minimize the cost of electricity, and consequently to make fusion energy more competitive.